Distribution Agreement

In presenting this thesis as a partial fulfillment of the requirements for a degree from Emory University, I hereby grant to Emory University and its agents the non-exclusive license to archive, make accessible, and display my thesis in whole or in part in all forms of media, now or hereafter now, including display on the World Wide Web. I understand that I may select some access restrictions as part of the online submission of this thesis. I retain all ownership rights to the copyright of the thesis. I also retain the right to use in future works (such as articles or books) all or part of this thesis.

Kelly Burke   April 18, 2012

Fast Mixing Reveals Two-state Folding of Apomyoglobin

by

Kelly Burke

Brian Dyer
Adviser

Department of Chemistry

Dr. Brian Dyer

Adviser

Dr. Khalid Salaita

Committee Member

Dr. Nitya Jacob

Committee Member

Ms. Brenda Harmon

Committee Member

2012

Fast Mixing Reveals Two-state Folding of Apomyoglobin

By

Kelly Burke

Dr. Brian Dyer

Adviser

An abstract of
a thesis submitted to the Faculty of Emory College of Arts and Sciences
of Emory University in partial fulfillment
of the requirements of the degree of
Bachelor of Sciences with Honors

Department of Chemistry

2012

Abstract

Fast Mixing Reveals Two-state Folding of Apomyoglobin
By Kelly Burke

The development of a novel fast mixer and its application to the study of protein folding is described. Construction of the mixer is simple and inexpensive, requiring no specialized equipment or techniques. The mixer is designed to achieve three-dimensional (3D), hydrodynamic focusing of the sample by a surrounding sheath solution. This focusing promotes rapid diffusional mixing between the two solutions. To characterize the mixer's performance, a sample flow rate calibration method utilizing the fluorescence decay of excited europium (Eu) microspheres was conducted. The achievable diffusional mixing times were also determined by observing the fluorescence quenching of fluorescein experiencing a rapid pH drop within the mixer. Mixing times as low as 111 μs were recorded. The mixer was then used to study the folding kinetics of apomyoglobin (apoMb) undergoing pH changes in the absence of buffer. Previous studies have demonstrated that apoMb populates four unique conformations –native, intermediate, extended, and unfolded – during its folding pathway. Under the conditions of this experiment, however, a two-state folding mechanism was observed. This suggests that these experimental conditions alter the relative energies of apoMb's conformations such that only two of them are appreciably populated.   It is possible that apoMb follows a folding pathway in which it reaches its lowest-energy native state without being trapped in relatively low-energy intermediate states.

Fast Mixing Reveals Two-state Folding of Apomyoglobin

By

Kelly Burke

Dr. Brian Dyer

Adviser

A thesis submitted to the Faculty of Emory College of Arts and Sciences
of Emory University in partial fulfillment
of the requirements of the degree of
Bachelor of Sciences with Honors

Department of Chemistry

2012

Acknowledgements

Table of Contents

List of Figures and Tables

1. INTRODUCTION

Protein folding is the process by which a protein, starting as a linear chain of amino acids, undergoes a series of conformational changes to ultimately assume a stable, 3D structure. This structure – called the native state – gives a protein its functional properties [1]. For example, members of the protein kinase C family contain catalytic domains that are uniquely shaped to bind only glycerol molecules, which these enzymes hydrolyze [2]. Because of the strong connection between protein structure and function, aberrations in a protein's native state can have deleterious biological effects, especially since proteins facilitate such vital processes as intracellular signaling, gene expression, and catalysis of biochemical reactions [1]. Several human neurodegenerative disorders – including Alzheimer's, Creutzfeldt-Jakob, Parkinson's, and Huntington's disease – have been linked to the aggregation of misfolded proteins [3]. Although the structure of a protein is known to depend on its amino acid sequence and solution conditions [4], the folding process by which it attains this structure is still not completely understood. Gaining more insight into the basic mechanisms of protein folding is critical to understanding certain diseases and cellular events. In addition, determining how particular amino acid sequences fold and contribute to protein structure could allow for enhanced engineering of proteins with useful properties [1, 5].

Protein folding research is complicated by the short timescales over which folding events occur. For instance, the development of secondary and tertiary structure may take place in microseconds or even nanoseconds [5]. In order to observe such fast events, new experimental techniques capable of initiating and monitoring folding processes on the same or even shorter timescales have been developed. Some of these techniques include temperature jump, photochemical triggering, and ultrarapid mixing of fluid samples [5, 6]. This thesis will focus on

ultra-rapid mixing and the development of a microfluidic mixing device to study the folding kinetics of a specific protein.

Microfluidics involves the control and analysis of micro-scale volumes of liquid in motion. An area of microfluidics that is of interest to protein folding research is the study of the interactions between two or more flowing liquids. The liquids being studied are often contained in devices called microfluidic mixers, which consist of two or more channels through which the liquids flow and eventually contact one another to initiate a chemical reaction (Figure 1). Typically, a sample solution is encountered from one or more sides by a sheath solution that mixes with the sample. The method of mixing that occurs between the sample and sheath solutions depends on the solutions' flow, which is characterized as either turbulent or laminar depending on the Reynolds number (R_e):

$$R_e = \frac{\rho v D_h}{\mu} \tag{1}$$

where ρ is the fluid density, v is the fluid velocity, μ is the fluid viscosity, and D_h is the hydraulic parameter, which depends on the diameter of the fluid channel [7]. An R_e value of 2300 or greater indicates turbulent flow, while a value lower than 2300 indicates laminar flow. Under turbulent flow conditions, particles of a liquid stream experience random motions such that the stream's velocity and pressure are not constant over time. These random motions ultimately allow for mixing between particles from different streams. Under laminar flow conditions, particles of a liquid stream travel uniformly at a constant velocity. Mixing then occurs by diffusion between streams that are in contact and travel parallel to one another [7, 8]. These contacting streams may exhibit a unique phenomenon called hydrodynamic focusing, which many microfluidic devices employ [9-16]. In this process, a sample solution is surrounded by a sheath solution that travels at a much higher velocity than the sample. As a

result, the sample stream is narrowed into a thin jet whose flow rate is accelerated to eventually

match and then exceed that of the sheath solution. This effect enhances the rate of diffusional

mixing between the sheath and sample solutions [8-9, 13].
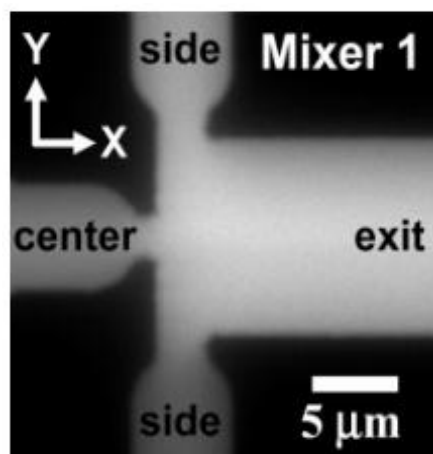
Figure 1. Example of a fast mixer, adapted from Yao and Bakajin, 2007 [14]. A sample solution
is ejected through a center channel, while a sheath solution is ejected through two opposing side
channels. The sheath solution meets the sample in the center, and the two solutions travel
alongside one another towards the exit. This particular design establishes a laminar flow of the
solutions and hydrodynamic focusing of the sample stream.

Fast mixers are useful in the study of protein folding because they can quickly perturb a

protein's solution environment to induce folding or unfolding of the protein. Often, a chemical

denaturant is mixed into or removed from a protein sample so that unfolding or folding,

respectively, is initiated and can be observed. One of the most common ways to infer protein

conformation is by fluorescence. For example, a protein may be probed with one or more

fluorescent molecules whose fluorescence quantum yield changes with perturbations in the

protein's structure. The protein itself may undergo changes in fluorescence with changes in its

structure if it contains fluorescent amino acids, which include tryptophan, tyrosine, and

phenylalanine [17]. A common method to capture and quantify the fluorescence of a protein

sample is fluorescence confocal microscopy. The major advantage of this technique over

conventional fluorescence microscopy is its ability to clearly resolve a single 2D section of a

sample by eliminating background fluorescence from other sections of the sample. Confocal miscroscopy can also achieve 3D imaging by simply overlaying several images of adjacent 2D sections. To reduce acquisition time while making 3D images, a spinning disk containing a series of pinhole apertures is often used [18-19]. All images collected in the experimental portion of this study were obtained by fluorescence confocal microscopy, which is described in more detail in the Materials and Methods section.

Several protein folding experiments utilizing fast mixers in conjunction with different optical techniques have already been conducted, and they report folding rates in agreement with those determined using other experimental techniques [15, 20-21]. However, the fabrication of mixing devices with enhanced mixing speed and efficiency is still being explored [10, 12-16, 22]. Major trends in improvement include reduced mixing time, sample consumption, and cost. Currently, microfluidic devices with experimental mixing times on the order of 10 µs [9, 11, 16] and theoretical mixing times as low as 1 µs [13] have been reported. These low mixing times were achieved with laminar-flow devices employing hydrodynamic focusing. To extend this improvement, an emphasis on 3D, rather than 2D, hydrodynamic focusing has been gaining interest [10, 15-16]. 2D-focusing devices bring the sheath solution into contact with only two opposite sides of the sample, thereby leaving areas of the sample that are above and below these sides unfocused and unable to directly mix with the sheath. Furthermore, these unfocused areas may contact the walls of the mixing device and therefore travel more slowly than parts of the sample not contacting the walls. This creates a gradient of flow velocities within the sample stream and may cause uncertainty in mixing time measurements. In contrast, 3D-focusing devices contact the sample from all sides with the sheath solution so that even diffusional mixing between the two liquids is achieved. Current 3D focusing devices are still limited in their ability

to experimentally achieve uniform mixing in a few microseconds or less. Silicon-based 3D mixers are further limited in their optical transparency – in general, only one side of the mixer admits light [7]. In addition, many 3D mixers are often complicated to construct, and only a few of them have been tested with a biological system, such as a protein or nucleic acid.

We have designed a 3D focusing microfluidic mixer to address these limitations. The mixer achieves uniform 3D focusing by completely surrounding the sample stream with a flowing sheath solution. This sheath solution hydrodynamically focuses the sample into a narrow jet so that rapid diffusional mixing between the solutions is initiated. The mixer is easily assembled with standard fittings and tubing, which are inexpensive and readily available. Because the capillaries are made of fused silica, all wavelengths of light are permissible through the mixer. This makes the mixer compatible with a variety of different optical spectroscopy techniques to observe reactions in the mixer. We emphasize confocal fluorescence detection, but Raman, infrared (IR), and ultraviolet-visible (UV-vis) absorption spectroscopy could also be used. Most significantly, the mixer is practical in protein folding studies. We demonstrate the mixer's utility in this regard by studying the folding and unfolding kinetics of apomyoglobin (apoMb).

ApoMb (myoglobin with the heme group removed) is a protein of particular interest in basic protein folding studies because of its simple structure. The protein consists of only 153 amino acids organized into 8 alpha helices labeled A-H [5]. The approximate structure of apoMb is shown in Figure 2, which depicts the native structure of horse heart myoglobin (used in the experiments of this thesis). In comparison, the native structure of apoMb has slight disorder in the C, D, and F helices [5]. Several studies to characterize apoMb's folding pathway have demonstrated that the protein can exist in one of four unique conformational states: the native

form (N), intermediate form (I), extended form (E), or unfolded form (U) [5, 23-25]. Between the N, I, and E forms, the N form has the most stable, compact structure, while the E form has the most loosely packed structure. Though they differ in overall compactness, each of these forms has hydrophobic core formed by the A, G, and H helices. This AGH core forms part of a hydrophobic pocket that contains the heme group of myoglobin. The remainder of the pocket is formed primarily by the B and F helices. The entire pocket becomes less structured as apoMb progress from N to I to E, though in the I form, much of the structure is still retained [5].

The unique conformations of apoMb may reflect intermediate states of apoMb's folding pathway [5]. Altering apoMb's structure from one state to another, then, may give insight into the protein's folding processes. One way to alter the structure of apoMb is through changes in the pH of the protein's environment. During acid denaturation, apoMb has been shown to transition between its structural states in two distinct folding events. At pH 7, apoMb exists in its N form. Between pH 5 and 3, the protein unfolds from its N form to I form due to the protonation of the imidazole side chains of three histidine residues (His24, His64, and His113). Below pH 3, the protein completely unfolds to its U form as the carboxyl groups on the side chains of a glutamate (Glu6) and an aspartate (Asp122) are protonated [26].
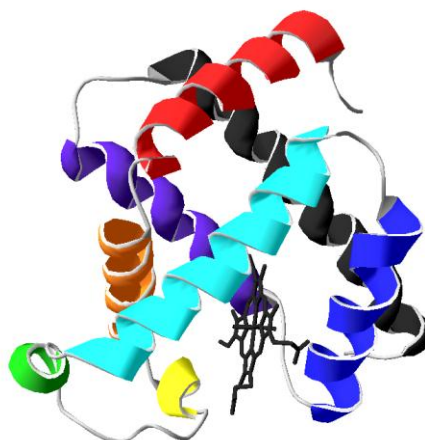
Figure 2. Structure of horse heart myoglobin from PDB file 3LR7. The helices are labeled A (red) through H (black). The A, G, and H helices form a compact, hydrophobic core that contains a heme group. ApoMb is prepared by removal of this heme group, which causes slight disorder in the C, D, and F helices as compared to myoglobin.

A useful monitor of these unfolding events is 1-anilinonapthalene-8-sulfonate (1,8-ANS), a fluorescent molecule that is capable of binding to apoMb's hydrophobic pocket (Figure 3). When 1,8-ANS is in aqueous solution, its fluorescence is quenched; however, when bound to the hydrophobic pocket of apoMb, its fluorescence is significantly increased. The binding of 1,8-ANS to apoMb becomes less efficient as the protein progresses from its N form (maximal binding) to its I and E forms (intermediate binding) and finally to its U form (no binding) [27]. Therefore, in our studies, the presence and degree of 1,8-ANS fluorescence will indicate whether apoMb is fully folded, partially folded, or completely unfolded.

Nonfluorescent   Nonfluorescent   Fluorescent in native
                                                 conformation

Removal of heme   Addition of 1,8-ANS
from myoglobin   to apoMb

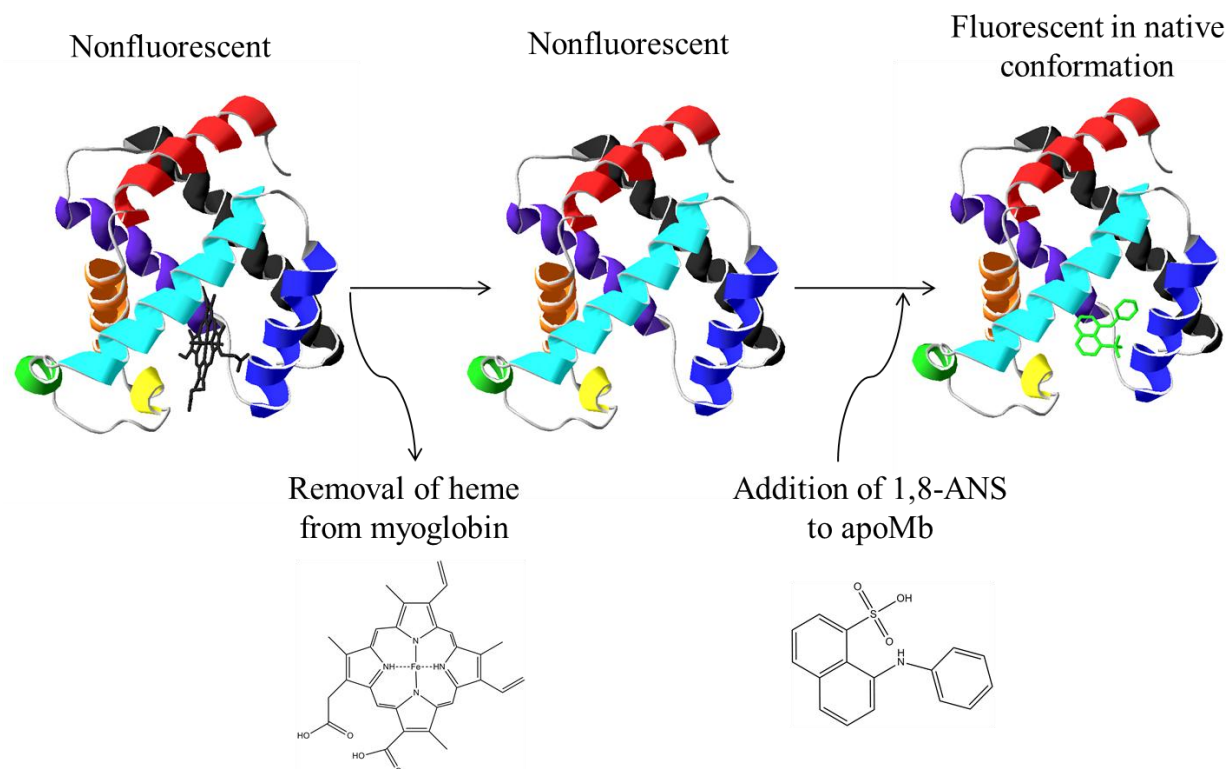**Figure 3**. Method of detection of protein folding. The heme group of myoglobin is removed, leaving the protein with an empty hydrophobic pocket to which 1,8-ANS binds. Upon binding, the fluorescence of 1,8-ANS dramatically increases. The binding is strongest when apoMb is in its N form. Detection of fluorescence indicates that apoMb is folded, and the absence of such fluorescence indicates that apoMb is unfolded.

In this thesis, the design and construction of a new microfluidic mixer is first described. The performance of the mixer is characterized by calibrating the sample flow rates and measuring the diffusional mixing times achievable. The sample flow rates were calibrated by observing the fluorescence decay of Eu microspheres in the mixer, and the diffusional mixing times were determined by observing the quenching of fluorescein fluorescence via a pH-jump in the mixer. The mixer's resolution of apoMb's folding pathway as the protein undergoes a pH-jump is then presented. Though this pathway has been investigated with other mixing devices [12, 21], the conditions of past experiments differ from those used here. Many studies alter the protein environment with buffered sheath solutions, but this experiment changes the pH of the protein by introducing non-buffered solutions. Such conditions create an interesting energy

landscape for apoMb folding that has not yet been observed. From the results of these studies, a

unique kinetic model for the folding and unfolding of apoMb is proposed.

2. MATERIALS AND METHODS

2a. Mixer Construction

Figure 4 illustrates the mixer components and overall design. The mixer was constructed

with standard plastic parts and 1/16" PEEK tubing supplied by Upchurch Scientific (Oak Harbor,

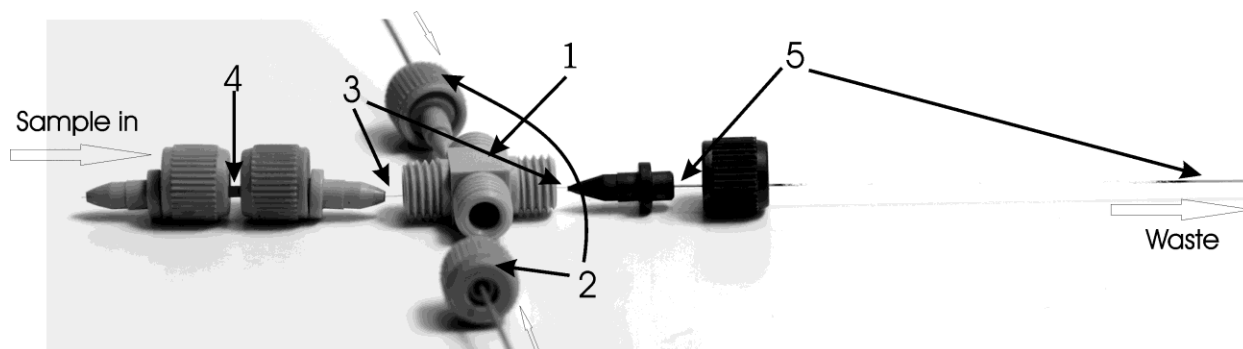WA) and fused silica capillaries supplied by Polymicro Technologies (Phoenix, AZ).

Figure 4. Design of mixer. The components included (1) MicroCross that holds 360-μm outer
diameter tubing and has a 150-μm through-hole (2) 1/32" PEEK tubing that has a 250-μm inner
diameter and carries sheath flow from HPLC pumps (3) Fused silica capillary for sample flow:
outer diameter - 90μm; inner diameter - 20μm (4) MicroTight tubing sleeve (5) Fused silica
capillary for sheath flow: outer diameter - 350 μm; inner diameter - 200 μm. All parts are
connected via fitting nuts and MicroFerrules with 0.025" diameters.

All parts of the mixer were connected by MicroFerrules and fitting nuts. The mixer

comprised two cylindrical, co-centered fused silica capillaries, the inner of which contained the

sample solution and outer of which contained the sheath solution. The sample and sheath

solutions were sent through the mixer by separate methods. Sample solutions were held in 1-mL

Tuberculin (Franklin Lakes, NJ) plastic syringes and were ejected by a KD Scientific (Holliston,

MA) continuous cycle syringe pump through approximately 25 cm of 1/32" PEEK tubing. The

tubing was attached to the mixer (at the "Sample in" end of Figure 4) such that the sample

solution was directed into the inner capillary. The inner capillary was held in a MicroTight

tubing sleeve to maintain its position within the mixer. The sleeve and inner capillary were connected to the central MicroCross. The inner capillary went through the MicroCross and into the center of the outer capillary, which was attached to the opposite side of the MicroCross.

The sheath solutions were ejected by two HPLC pumps. The reported sheath flow rates reflect the combined delivery of the two pumps, as each pump delivered sheath solutions at half the reported rates. Each HPLC pump sent liquid through separate metal tubes to reach a baffle, where the sheath solutions delivered by each pump met. From the baffle, the total sheath solution volume traveled through a T-junction and was divided into two separate channels made of approximately 75 cm of 1/32" PEEK tubing. The channels (indicated by (2) in Figure 4) were directed into opposite sides of the MicroCross.

As described above, the outer capillary holding the sheath solution encompassed the inner capillary holding the sample solution (Figure 5). The outer capillary had a 350-μm outer diameter (OD) and 200-μm inner diameter (ID), and the inner capillary had a 90-μm OD and 20-μm ID before the narrowed tip area. The outer and inner diameters at the tip of the inner capillary were reduced to 20 μm and 8 μm, respectively. This narrow tip was produced by a simple pulling method (Figure 6). First, the capillary was attached to a plastic 50-mL cylindrical tube filled with 45 mL of water. The capillary was then suspended from a support stand and melted with a propane pencil flame burner torch. The narrow tip, along with the 3D focusing of the sheath solution, allowed formation of a thin sample jet that was 2-5 μm in diameter.
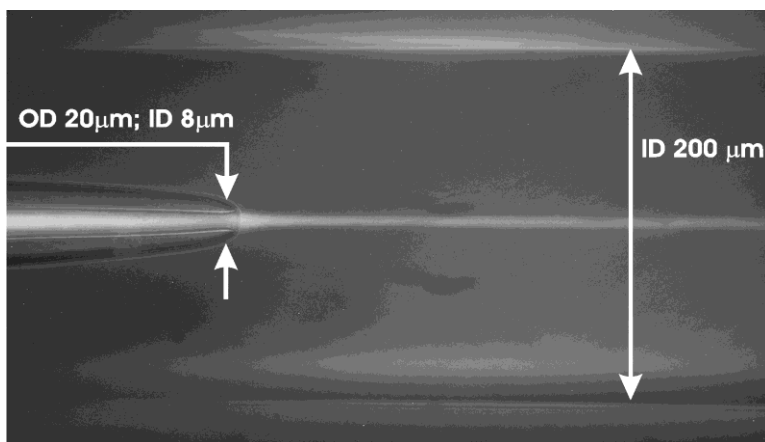
Figure 5. Capillary flow system. The sample flows from left to right through the inner capillary, which at its tip has an outer diameter of 20 μm and inner diameter of 8 µm. The sheath solution flows from left to right through the outer capillary, which has an inner diameter of 200 µm. The tapered capillary tip and 3D focusing by the sheath solution create a narrow sample jet that is 2-5 µm in diameter. A laminar flow of the sample is established and rapid mixing occurs via diffusion. Pictured are Eu beads flowing through the channel. The sample flow rate is 0.025 µL/min, and the sheath flow rate is 100 µL/min.

Figure 6. Pulling of the inner capillary. The inner capillary is attached to a conical tube containing 45 mL of water and is then placed onto a support stand. The tube pulls the capillary, which is melted with a propane pencil flame burner torch.

The mixer was mounted onto an Applied Scientific Instrumentation (Eugene, OR) MS-2000 automated stage using Newport (Irvine, CA) miniature optical rails and lens mounts. A 3-in rail and a 6-in rail were attached at their ends. The 3-in rail was fixed to the stage, while the 6-in rail was placed over the objectives. Two fixed-position lens mounts were attached to the 6-in rail, and the capillary system was placed within these lens mounts (Figure 7). The stage was attached to an Olympus (Center Valley, PA) IX81 microscope, and the capillary system was rotated around the connection between the 3-in and 6-in rails to place the mixer directly onto the microscope's objective for viewing.
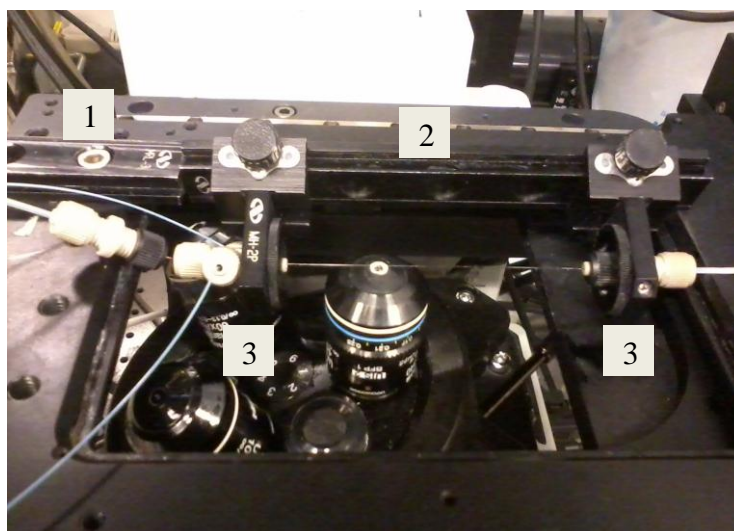
Figure 7. Set-up of microfluidic mixer over microscope objective. (1) A 3-in optical rail is connected to (2) a 6-in optical rail. The mixer is held between (3) two lens mounts.

2b. Sample Preparation

Three different sample solutions were used in the mixer: Eu micospheres, fluorescein, and apoMb. Before use, all sample solutions were filtered with 0.2-μm PTFE filters supplied by Nalgene (Rochester, NY). All sheath solutions were filtered with 0.22-μm PES filters supplied by Corning (Lowell, MA). Details of each sample preparation are given below.

Europium microspheres

Eu carboxylate-modified microspheres 0.04 μm in size were purchased from Invitrogen (Grand Island, NY) and used without further modification.

Fluorescein

Fluorescein was purchased from Sigma-Aldrich (St. Louis, MO). A solution of fluorescein was prepared by dissolving it in deionized (DI) water and then adding NaOH to the solution to reach a pH of approximately 8, at which the quantum yield of fluorescein fluorescence reaches a maximum. The concentration of fluorescein was determined using the extinction coefficient of 80,000 $M^{-1}cm^{-1}$ at 488 nm [28].

Apomyoglobin

Equine skeletal muscle myoglobin was purchased from Sigma-Aldrich. A solution containing 5 mg of protein/mL of deionized water was prepared. Myoglobin was precipitated from this solution by adding ammonium sulfate to 68% saturation at room temperature. The sample was dialyzed overnight against deionized water using regenerated cellulose dialysis tubing by Fisherbrand (Pittsburg, PA). ApoMb was prepared from this sample according to a modification of the procedure of Adams [29]. In this modification, the diethyl ketone extraction and dialysis were performed twice to improve sample purity. In addition, apoMb was dialyzed against deionized water only. Details of the procedure are given below.

The myoglobin solution was placed into glass centrifuge tubes and cooled over ice to 0°C. The pH of the solution was lowered to 3.5 by addition of 1-M HCl. This unfolds myoglobin so that its heme group is accessible for removal by extraction. An extraction was

performed by adding diethyl ketone to the myoglobin solution in a 1:1 volume ratio and then

shaking the mixture for one minute. The mixture was also spun in a centrifuge at 0°C for 1

minute at 5000 rpm. The total mixing process partitioned the solution into an organic layer of

diethyl ketone on the top and an aqueous layer of DI water on the bottom due to the lower

density of diethyl ketone versus DI water. The organic layer contained the heme molecules

removed from myoglobin, and the aqueous layer contained the heme-free protein: apoMb. The

upper layer containing heme was discarded, and the lower layer containing apoMb was further

modified. NaOH was added to the apoMb solution until its pH reached between 5.5 and 6 in

order to reestablish the protein's folded conformation. The apoMb solution was dialyzed

overnight to remove excess diethyl ketone and was then stored at -80°C in 0.5-mL volume

samples. For experimentation, the individual samples were thawed from -80°C to room

temperature, and DI water was added to the samples to reach the desired apoMb concentration.

The concentration of apoMb was determined using the extinction coefficient of 15570 $M^{-1}cm^{-1}$ at

280 nm [29].

To observe apoMb under the microscope, the protein was probed with 1,8-ANS, which

was also purchased from Sigma-Aldrich. A solution of 1,8-ANS was prepared by dissolving the

compound in DI water. The 1,8-ANS solution was added to apoMb to make samples with a 1,8-

ANS: apoMb concentration ratio of approximately 1:1. The concentration of 1,8-ANS was

determined using the extinction coefficient of 5000 $M^{-1}cm^{-1}$ at 350 nm [30].

2c. Image Collection and Analysis

Each sample described above was observed by confocal fluorescence imaging using an

Olympus IX81 motorized inverted microscope. In the standard set-up of this confocal

microscope, excitation light travels through a narrow pinhole aperture and then reaches the

sample. The pinhole reduces the excitation light to a single illumination spot on the sample.
Fluorescent light emanating from this illumination spot is then directed through a second pinhole
and eventually reaches a detector. The second pinhole is placed at a plane before the detector
where both this pinhole and the illumination spot of the sample are in focus. Hence, only in-
focus light coming from the focal plane of the sample is detected; out-of-focus background light
that may come from layers above or below the focal plane of the sample is rejected [18-19]. The
standard confocal set-up was used to collect 2D images.

3D images, which were projections of several 2D images, were collected with a spinning
disk in place of the two pinhole apertures in the standard set-up. The spinning disk contains a
series of equally-spaced pinhole apertures having the same diameter. Excitation light passes
through the disk and illuminates several separate spots of the sample. Light from these spots on
the sample then passes back through the pinholes of the disk, and the in-focus image of each
illuminated spot is located at a specific pinhole. Again, this method of focusing with pinholes
eliminates out-of-focus light. As the disk rotates, the entire field of view is covered with light so
that a full image of the sample can be formed. Because multiple spots of the sample are
illuminated simultaneously, images can be collected more quickly with the spinning disk than
without it [18-19]. This allows rapid collection of 2D images that can be overlaid to make a 3D
image.

Images were analyzed using Igor Pro Software. For a given image, the sample
fluorescence intensity was plotted against pixels along the length of the image. To make this
plot, the sample fluorescence intensity and the background signal intensity were integrated over a
specific number of pixels across the width of the image at each pixel along the length of the
image. The background signal was subtracted from the sample signal, which was then plotted

against pixels along the length of the image. The data were finally fit to an appropriate function in Igor Pro. For instance, consider a sample stream that was 20 pixels in width and 800 pixels in length. The intensity of the sample stream's fluorescence, as well as that of the background signal, would be integrated over 20 pixels in width for each of the 800 pixels in length. Next, the integrated background intensity at each pixel would be subtracted from that of the fluorescence intensity. The background-subtracted fluorescence intensity would be plotted against the 800 pixels along the length of the image, and the data would be fit to a function that properly described the behavior of the fluorescence across those 800 pixels.

2d. Experimental Designs and Procedures

Each sample described in section 2b. was used to perform a different experiment in this study. Eu microspheres were used to determine the time resolution of the mixer; fluorescein was used to calibrate the time required for proton diffusion into the sample stream; and apoMb was used to study the kinetics of protein folding due to a pH-jump. The purpose, set-up, and specific conditions of each experiment are described below. All filters, lenses, and mirrors described in the optical set-ups of the experiments were purchased from Semrock (Rochester, NY).

Flow Rate Calibration

The flow rate calibration was conducted in order to determine the time resolution of the mixer under certain experimental conditions with respect to the ejected sample and sheath flow rates. The time resolution indicates the amount of time required for a sample stream to travel across a single pixel along the length of an image for a given sheath flow rate and at a certain magnification. Given the proper conversion factors, the time resolution could theoretically be determined by converting the sample flow rate from mL/min into seconds/pixel. However,

although the sample is ejected at a known rate by the syringe pump, this rate changes once the sample exits the inner capillary due to hydrodynamic focusing by the surrounding sheath solution. As described in the introduction, the sample flow rate is accelerated by the faster-moving sheath solution. Determining the time resolution of the mixer therefore required an experimental calibration.

First, the fluorescence decay time of the Eu microspheres needed to be determined. This was done by exciting a sample of Eu microspheres with a 351-nm laser that pulsed with a repetition rate of 1 kHz. The Eu fluorescence that was perpendicular to the incident beam was focused onto a monochromator. Prior to striking the monochromator, the fluorescence was filtered such that only light at 610 nm, which is the fluorescence wavelength of Eu microspheres reported by the manufacturer, would reach the monochromator. From the monochromator, the fluorescent light was directed to a photomultiplier tube (PMT). The PMT signal was collected by an oscilloscope, which averaged about 1000 laser pulse signals. The fluorescence intensity signal was plotted against time, and the data past the initial laser spike signal was fit to a single exponential function:

$$y = y_0 + Ae^{-\lambda x} \tag{2}$$

where y_0 is the limit of the signal intensity as time approaches infinity, A describes the maximum signal intensity at time 0, and λ (lambda) is the decay constant. The signal decay time (τ), which is the time required for the signal intensity to reach $\frac{1}{e}$ of its starting intensity, was calculated by taking the inverse of the decay constant:

$$\tau = \frac{1}{\lambda} \tag{3}$$

To calibrate the sample flow rates and thus determine the time resolution of the mixer, the Eu microspheres' fluorescence decay was observed within the mixer. Eu microspheres were

sent through a sheath solution of DI water. The Eu microspheres were ejected at a constant rate of 0.1 μL/min, while the DI water was ejected at rates of 0.25, 0.50, 0.75, and 1.00 mL/min. Observing the Eu microspheres' fluorescence in the mixer required a unique optical set-up in the microscope. A Newport (Irvine, CA) UV diode laser emitting 375-nm light with 16-mW power was used to excite the sample of flowing Eu microspheres. The 375-nm laser beam passed through a 300-390 nm band pass filter, then a cylindrical lens with a 100-mm focal point, and finally a 50-μm slit before entering the side port of the microscope. The cylindrical lens focused the laser beam into a narrow line, and the slit reduced this line to a maximum width of 50 μm. The narrowed beam then refracted through an internal prism of the microscope and passed through a dichroic mirror (transmission: 325-480 nm, reflection: 520-610nm) to reach the objective. All flow rate calibration experiments were performed using the 40X water objective. The laser beam – appearing as a narrow line – hit the mixer capillary system and excited the Eu microspheres flowing through the mixer at a single point along their trajectory. The fluorescence of the excited microspheres transmitted back through the objective, reflected off the dichroic mirror, and passed through a 609-nm short-pass filter to ultimately reach the camera. 2D images of the Eu microspheres' fluorescence were captured.

The time resolution was finally determined by comparing the measured fluorescence decay of the Eu microspheres in seconds to their observed fluorescence decay within the mixer in pixels along an image. Again, the Eu microspheres were excited by a laser at a single point along their trajectory. At this point, the Eu microspheres began to fluoresce. As they moved away from this point, their fluorescence decayed over time. For a given image collected in a calibration experiment, the fluorescence signal intensity versus pixel along the image was plotted. The data were fit to Equation 2, and the decay of the signal in pixels was calculated with

Equation 3. The time resolution for specific flow rate conditions in the mixer was then obtained

by dividing the previously determined decay in seconds by the observed decay in pixels.

Diffusional Mixing Time Calibration

The final apoMb experiments involved the diffusion of protons into the sample stream to

change the pH of the sample. With the pH-change, changes in protein conformation were

expected. The raw data for apoMb folding times due to pH changes therefore included both the

time necessary for proton diffusion to occur and the time for apoMb to fold or unfold. To

separate these times, the time required for proton diffusion into a sample had to be determined.

For this calibration, a pH-jump of fluorescein was performed in the mixer. Fluorescein is a

fluorescent dye molecule whose fluorescence quantum yield depends strongly on pH. At a high

pH (approximately 8-9), fluorescein exhibits highly intense fluorescence; at a low pH

(approximately 2-3), this fluorescence is quenched [28].

A new optical set-up was required to observe the fluorescein fluorescence within the

mixer. An HBO mercury (Hg) short-arc lamp from Osram (Danvers, MA) was used to excite

fluorescein, which absorbs maximally at 488 nm and fluoresces at approximately 525 nm [28].

The lamp light passed through a 482 ± 12-nm band-pass filter and then reflected off a 488-nm

RazorEdge dichroic mirror. Light directed towards the mixer passed through a 488-nm long-

pass filter. The light then passed through the objective. All fluorescein experiments were

performed using the 100X oil objective. The light reached the mixer and excited the fluorescein

sample. Unlike the flow rate calibration experiments, which used a single line of laser

excitation, the fluorescein experiments were conducted by illuminating the entire sample flow

through the mixer with excitation light. Fluorescence from the fluorescein passed back through

the objective and 488-nm long-pass filter. The fluorescence then transmitted through the 488-nm

dichroic mirror to reach a different mirror that directed the fluorescence to the camera. 2D

images of the fluorescein fluorescence were captured.

The diffusional mixing calibration experiment was conducted by sending a sample stream

of fluorescein at a pH of 8 through a surrounding sheath layer of hydrochloric acid (HCl) at a pH

of 2. The sample flow rate was at 0.1 μL/min, and the sheath flow rate was 0.75 mL/min. The

proton gradient between the sheath and sample solutions caused protons from the sheath to

diffuse into the sample. This lowered the pH of the fluorescein sample stream and therefore

caused the fluorescein fluorescence to quench. The fluorescence quenching was assumed to be

diffusion-limited, meaning the time over which quenching occurred was equal to the time

required for proton diffusion. This time was determined by first plotting the fluorescein

fluorescence intensity versus pixel along the length of the image. Similar to the Eu experiments,

the data were fit to Equation 2, and the decay in pixels was determined with Equation 3. This

decay in pixels was multiplied by the appropriate time resolution (determined from the flow rate

calibration experiments) in order to determine the decay in seconds. This decay in seconds

corresponded to the time required for proton diffusion.

ApoMb Folding

As described in the introduction, the conformation of apoMb is highly sensitive to pH

[12, 21, 26]. The pH of apoMb samples in the mixer was lowered or raised to induce unfolding

or folding, respectively. Unfolding experiments were conducted by flowing apoMb samples at a

pH of approximately 5.5 – 6 through a sheath of HCl at a pH of 2. Folding experiments were

conducted by first adding HCl to the apoMb samples and then flowing these samples through a

sheath of DI water. A control study was also performed by flowing unaltered apoMb samples through DI water. The sample flow rate was 0.1 µL/min, and the sheath flow rate was 0.2 mL/min.

An optical set-up similar to that used for observing fluorescein was used to observe apoMb. This observation relied upon viewing the fluorescence of 1,8-ANS, which was added to the apoMb samples as described in section 2b. Excitation light from the same Hg lamp passed through a 390 ± 40-nm band-pass filter, then reflected off a 405-nm RazorEdge dichroic mirror, and finally passed through a 405-nm long-pass filter and the objective. All apoMb experiments were performing using the 40X water objective. The light reached the mixer and excited the fluorescence of 1,8-ANS in the sample. Fluorescence from the 1,8-ANS passed back through the objective and 405-nm long-pass filter. The fluorescence then transmitted through the 405-nm dichroic mirror to reach a different mirror that directed the fluorescence to the camera. Whereas 2D images were collected for the flow rate and proton diffusion calibration experiments, 3D confocal images requiring the spinning disk were collected for the apoMb experiments.

The apoMb folding images were analyzed by plotting the sample fluorescence intensity against the pixel along the image. Again, the data were fit to Equation 2, and the change in fluorescence signal in pixels was determined with Equation 3. The change in fluorescence signal was converted from pixels to seconds by multiplying the pixel change by the appropriate time resolution. The resultant decays in seconds corresponded to the time required for apoMb folding or unfolding.

3. RESULTS AND DISCUSSION

3a. Flow Rate Calibration

The single exponential fit to the fluorescence decay of the Eu microspheres over time followed the equation: $y = 0.071284 + 0.85916e^{-1824.2x}$ (Figure 8). Given this equation, the fluorescence decay time of the Eu microspheres was found to be 548 µs.
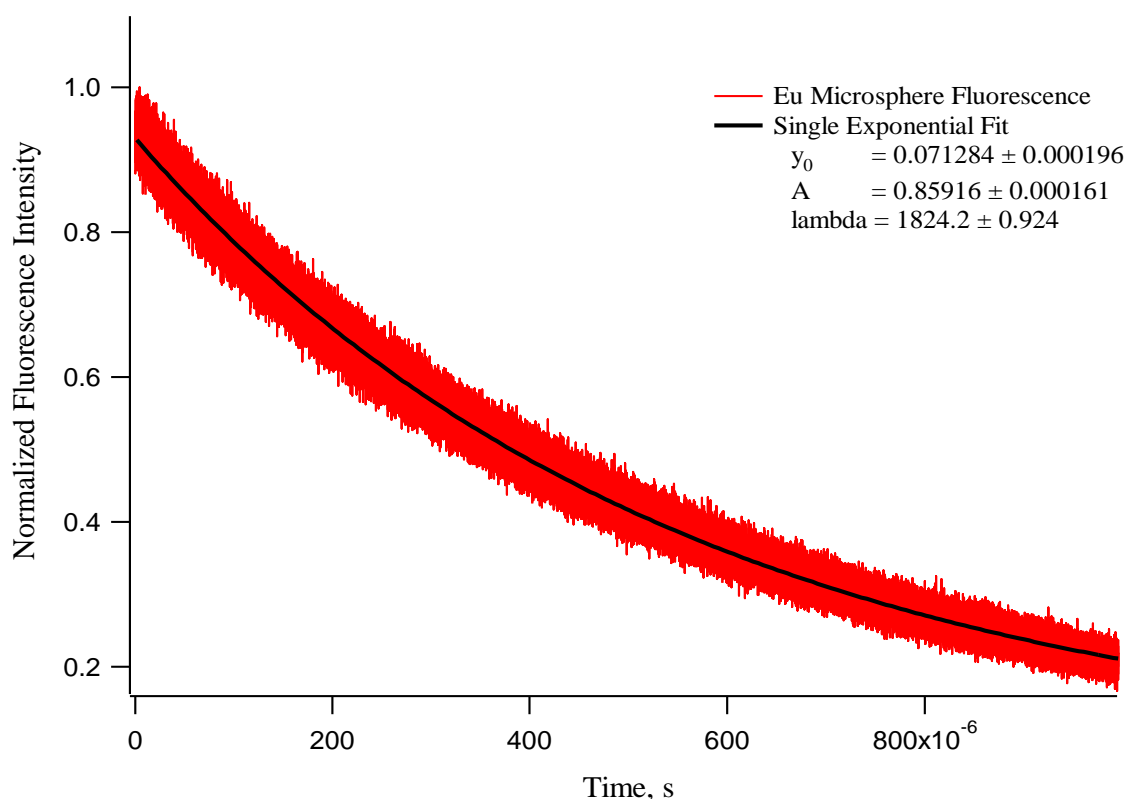

Figure 8. Fluorescence decay of Eu microspheres over time. The data were fit to a single exponential: $y = 0.071284 + 0.85916e^{-1824.2x}$. The decay time was 548 µs.

After measuring the decay time of the Eu microspheres, the time resolution of the mixer could be determined from observing the fluorescent signal of Eu microspheres traveling through the mixer (Figure 9). As previously described, the intensity of the fluorescence decay signals were integrated, and these signal intensities were plotted versus pixel along the length of an image. The analysis for the time resolution is demonstrated in Figure 10.
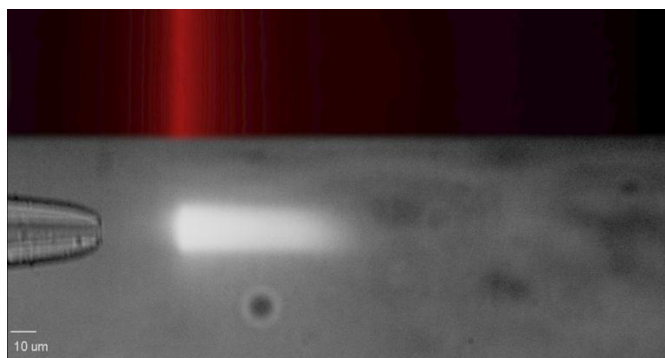
Figure 9. Single-point laser excitation of Eu microspheres flowing through the mixer. The microspheres exiting the inner capillary are excited by a laser focused on a narrow line across the flow channel. The microspheres begin to fluoresce, and as they move away from the excitation point, the intensity of their fluorescence decreases.
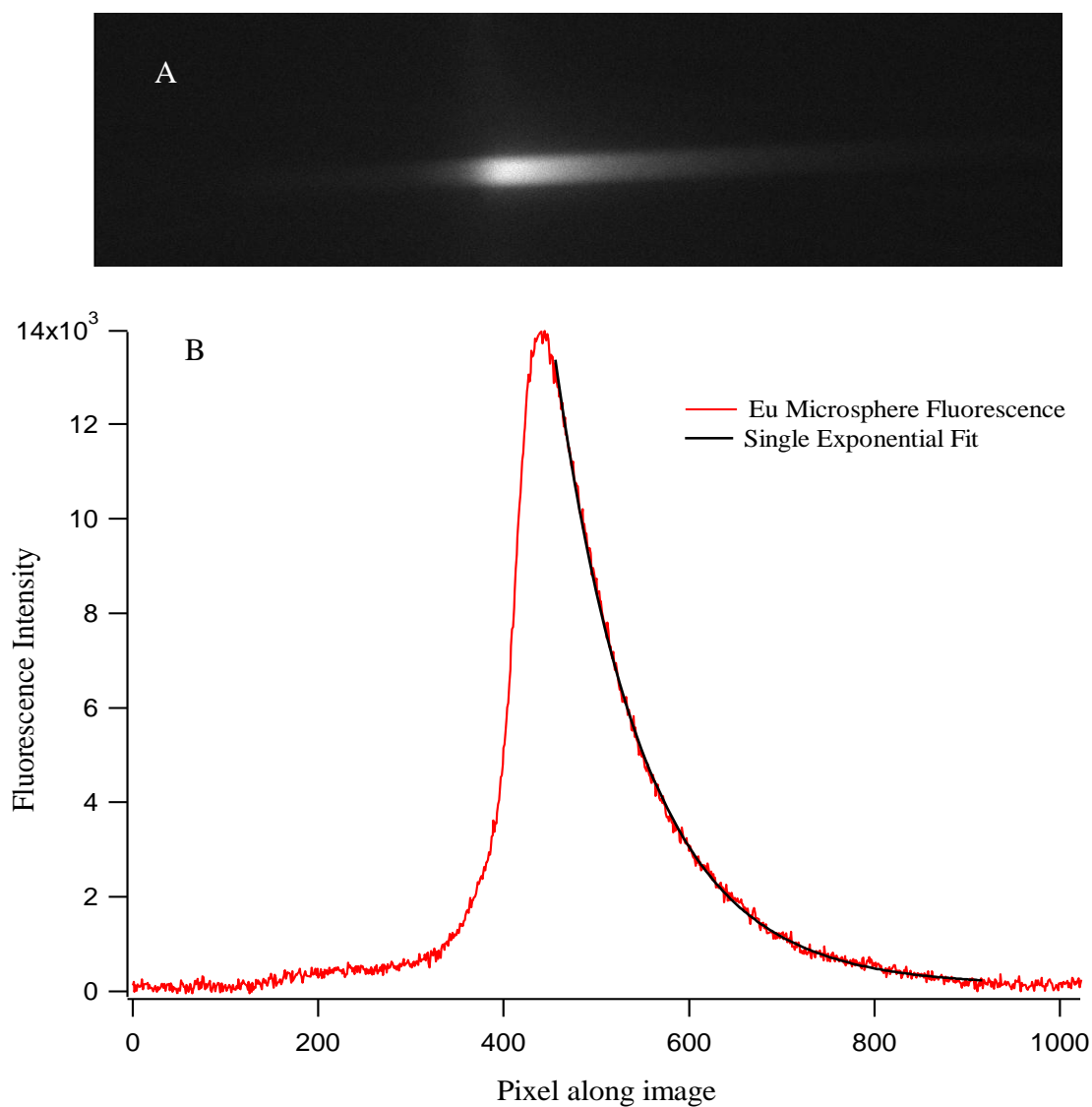
Figure 10. Example of time resolution data analysis. (A) 2D image of Eu microsphere fluorescence decay within the mixer. (B) Trace of fluorescence intensity per pixel along (A). The data is fit to a single exponential function from which the fluorescence decay in pixels can be calculated. The time resolution is found by dividing the Eu microsphere decay time in seconds by this decay in pixels.

As sheath flow rate increased, the sample flow rate also increased, and the experimental time resolution decreased (Table1). This trend is expected since a sample traveling at a faster rate will move across a given distance, or a given number of pixels, in fewer seconds. To further assess whether the experimental time resolution is reasonable, a theoretical time resolution that assumes all liquid in the mixer travels at the rate of the sheath solution was calculated. Since the rate of the sample should actually exceed that of the sheath solution, this theoretical time resolution should serve as an upper-bound to the experimental time resolution. The theoretical time resolution was calculated by converting each sheath flow rate (in mL/min) into a time resolution (in μs/pixel). First, the sheath flow rates are inverted so that time is in the numerator, and volume is in the denominator. Time is converted from min to μs by simply multiplying by 6 x 10^7 μs/min. Volume is converted to pixels by dividing by the cross-sectional area of the outer capillary (since the volume being considered is assumed to span this entire area) and then multiplying by the number of pixels per unit length across the microscope image. The calculation, with certain parameters and their units specified, is summarized by:

$$\frac{time, \ min}{volume, \ mL} * \frac{6*10^7 \mu s}{min} * \frac{mL}{cm^3} * cross - sectional \ area, cm^2 * \frac{length \ of \ image, \ cm}{number \ of \ pixels \ along \ image} = \frac{\mu s}{pixel}$$

Based on this theoretical calculation, the experimental time resolution was assumed to be inversely proportional to sheath flow rate. The experimental time resolution, however, was expected to follow a function with a different curvature and position than that followed by the theoretical time resolution. Presumably, the experimental time resolution should have lower values, since the flow of the sample in the center of the capillary is expected to travel more

quickly than the average flow velocity. Therefore, the experimental time resolution data was fit

to an inverse function with adjustable parameters (manually programmed into Igor Pro). The

function was given by:

$$y = c_1 + c_2 \left(\frac{1}{x}\right) \tag{4}$$

where c_1 is a factor that adjusts the y-position of the function, and c_2 is a factor that adjusts the

curvature of the function.

The experimental data fit well to an inverse function with the formula $y = 1.1928 +$

$1.1518 \left(\frac{1}{x}\right)$. However, the data points are not lower than those determined from the theoretical

calculation (Table 1, Figure 11).

Table 1. Theoretical and Experimental Time Resolution of the Mixer at 40X Magnification for
Different Sheath Flow Rates

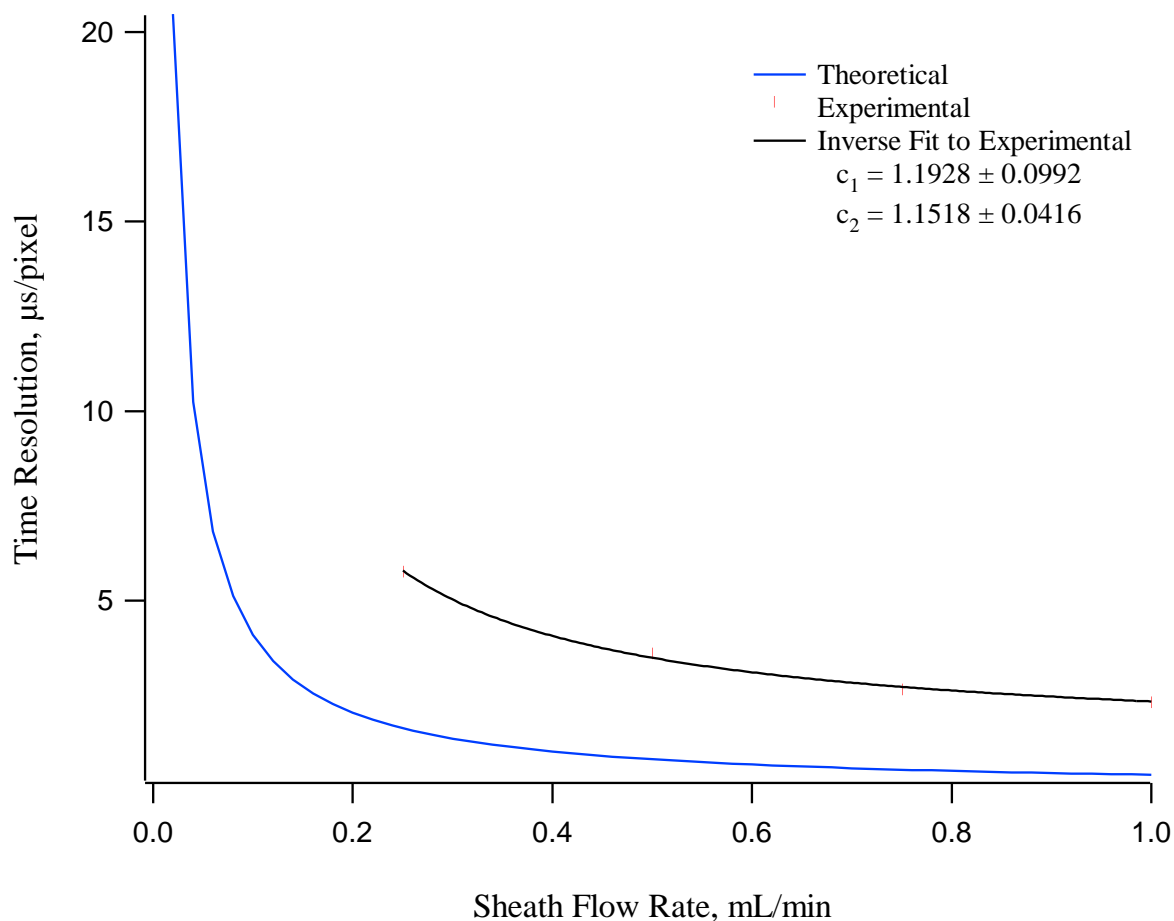| Sheath Flow Rate, mL/min	Theoretical Time Resolution, µs/pixel	Experimental Time Resolution, µs/pixel
0.25	1.64	5.77
0.50	0.819	3.61
0.75	0.546	2.66
1.00	0.410	2.33

Figure 11. Time resolution of microfluidic mixer at 40X magnification against corresponding sheath flow rate while the sample was ejected at a constant rate of 0.1 µL/min. The experimental data were fit to an inverse function: $y = 1.1928 + 1.1518 \left(\frac{1}{x}\right)$.

The theoretical time resolution points that correspond to the experimental points are faster by a factor of approximately 3.5 to 5.7, and this factor increases as the sheath flow rate increases. Error in the data may have resulted from the sample stream of Eu beads being out of focus. The sample stream is cylindrical, so if the top or bottom (rather than the center) of the sample stream were observed, then the apparent number of pixels over which the fluorescence signal decayed would be fewer. This would make the calculated time resolution greater since it involves time divided by pixels.

The sample stream could have been out of focus if the inner capillary was not centered directly within the outer capillary. This error may have occurred with the current set-up of the system. When the mixer was rotated so that it rested on top of the objective, the MicroTight tubing sleeve that holds in the inner capillary was bent because it was blocked by the microscope stage (Figure 12). Bending the sleeve may in turn have bended the inner capillary, and therefore the sample stream, so that neither was directed straight through the center of the outer capillary. This would have caused uneven focusing of the sample stream. To avoid bending the inner capillary, a stage with an opening where the MicroTight sleeve can rest without being bent should be used. Also, to establish a better focus at the center of the sample stream, the spinning disk of the microscope should be utilized. By eliminating background fluorescence, the spinning disk allows clearer identification of specific parts of the sample stream. With the disk in place, the center of the stream could be identified and an image of it could be collected. If necessary, the disk could be removed to increase the fluorescence signal right before capturing the image.
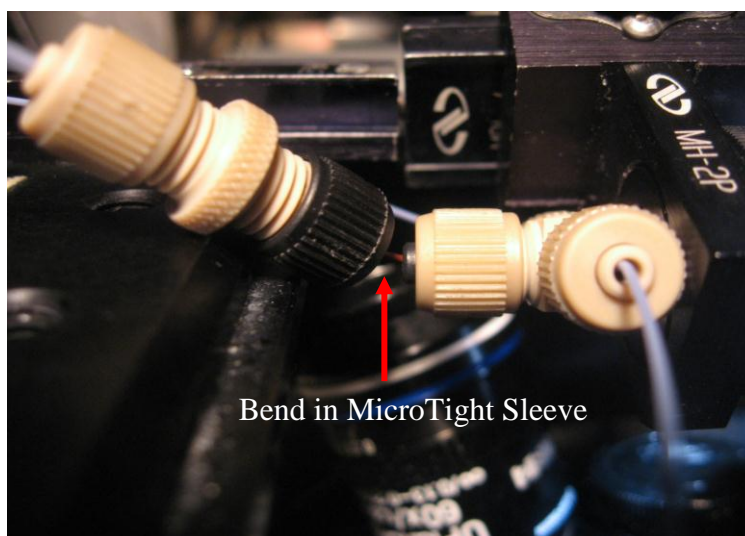

Figure 12. Bending of the mixer over the microscope stage. The MicroTight sleeve is bent and may misdirect the inner capillary away from the center of the outer capillary.

Although seemingly inaccurate, the experimental time resolution was used to analyze

subsequent data. The following times reported for diffusional mixing and protein folding

reactions in the mixer may therefore give upper limits to the actual times being observed.

3b. Diffusional Mixing Time Calibration

An example of fluorescein fluorescence quenching due to a decrease in the pH of a

fluorescein sample is demonstrated in Figure 13. The fluorescence intensity was plotted versus

pixel along the length of the image, beginning at the inner capillary tip, where the fluorescein

first encounters the sheath solution of HCl. The data was fit to a single exponential function

(Figure 14).
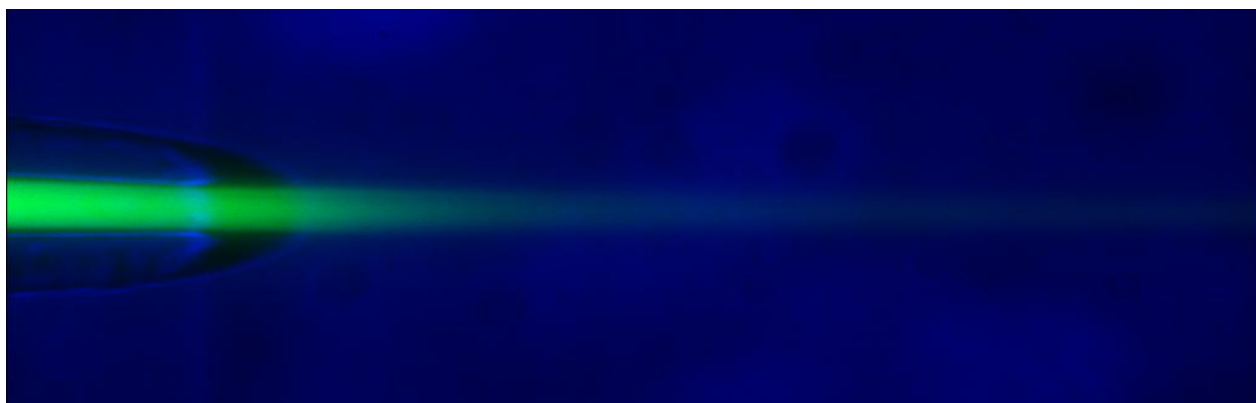
Figure 13. Quenching of fluorescein fluorescence as the pH of the fluorescein is decreased due
to the diffusion of protons from an HCl sheath layer into the fluorescein sample stream. The
fluorescein fluorescence is shown as a green trace against a blue background. The concentration
of fluorescein was 10-μM. The fluorescein sample was at an initial pH of 8, and the HCl sheath
was at a pH of 2. The fluorescein sample was ejected at 0.1 μL/min, and the HCl sheath was
ejected at 0.75 mL/min.

Figure 14. Decay of fluorescein fluorescence intensity as a sample of 10-µM fluorescein at pH 8 travels at 0.1 µL/min through a surrounding sheath solution of HCl at pH 2 traveling at 0.75 mL/min.
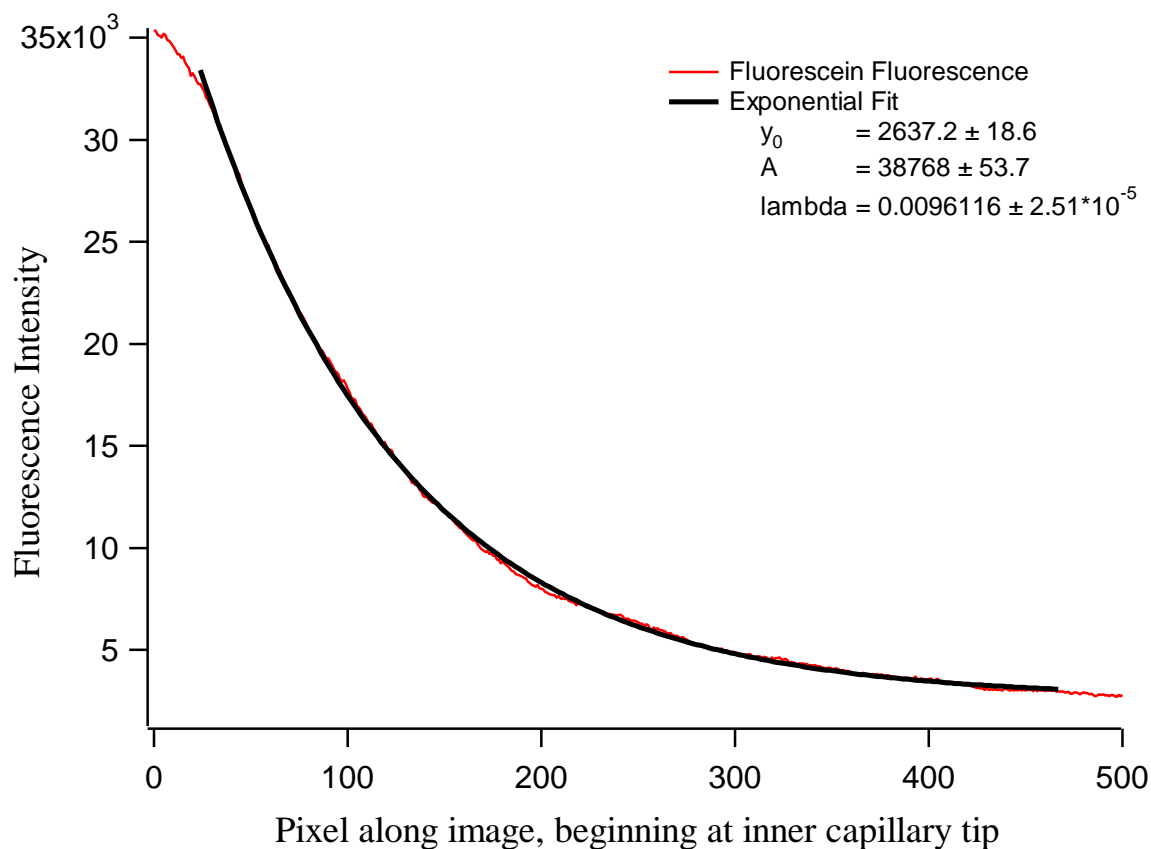
The exponential fit of Figure 12 has a decay of 104 pixels. The sheath flow rate was 0.75 mL/min, which at 40X magnification, gives a time resolution of 2.66 µs/pixel (Table 1). However, since the fluorescein experiments were conducted under the 100X objective, the time resolution can be decreased by a factor of 2.5. This results in a time resolution of 1.06 µs/pixel. Multiplying this time resolution by the pixel decay gives a proton diffusion time of 111 µs. Other studies have reported proton diffusion times about an order of magnitude lower than this time [9, 11-12, 14, 16]. The large error most likely stems from error in the calibration data. The fluorescein experiments may also have been out-of-focus like the Eu microsphere experiments

may have been. If the theoretical time resolution data is used, the proton diffusion time is approximately 22.7 μs, which agrees well with the other reported values. The actual diffusional mixing time achievable by our mixer may be even faster than those values, since the experimental time resolution is expected to be lower than the theoretical. Nonetheless, the ensuing results are based on using the observed mixing time of 111 μs.

3c. ApoMb Folding

Three different experiments with apoMb were conducted to understand its folding kinetics. For all experiments, apoMb was probed with 1,8-ANS in an approximate 1:1 concentration ratio: the concentration of apoMb was 160 μM and that of ANS was 200 μM. To measure the rate of unfolding, the apoMb: 1,8-ANS sample at a pH of approximately 5.5 was sent through a sheath solution of HCl at a pH of 2. To measure the rate of folding, the sample with 1-mM HCl added (final pH was approximately 3) was sent through a sheath solution of NaOH at a pH of 7. A control experiment in which the sample at a pH of 5.5 was sent through a sheath solution of DI water was also conducted. The sheath flow rate for all experiments was 0.20 mL/min. At this sheath flow rate and under the 40X water objective (used for all apoMb experiments), the time resolution of the mixer was 6.95 μs/pixel. This was determined from the inverse fit function to the experimental time resolution data.

The results of the apoMb experiments are shown in Figure 15. In the unfolding experiment, the apoMb:1,8-ANS sample's fluorescence intensity decreased as protons from the HCl sheath solution diffused into the sample stream. In the refolding experiment, the opposite effect was observed: the sample's fluorescence intensity increased as protons diffused out of the sample stream. The unfolding and refolding data fit well to single exponential functions, which gave reaction times of 607 μs and 172 μs for unfolding and refolding, respectively (Table 2).

Because these times are longer than the diffusional mixing time, we can assume that they reflect

the kinetics of apoMb folding. The control experiment demonstrated a gradual decline in

fluorescence intensity, which may be described by diffusion of apoMb with 1,8-ANS bound out

of the sample stream over time.
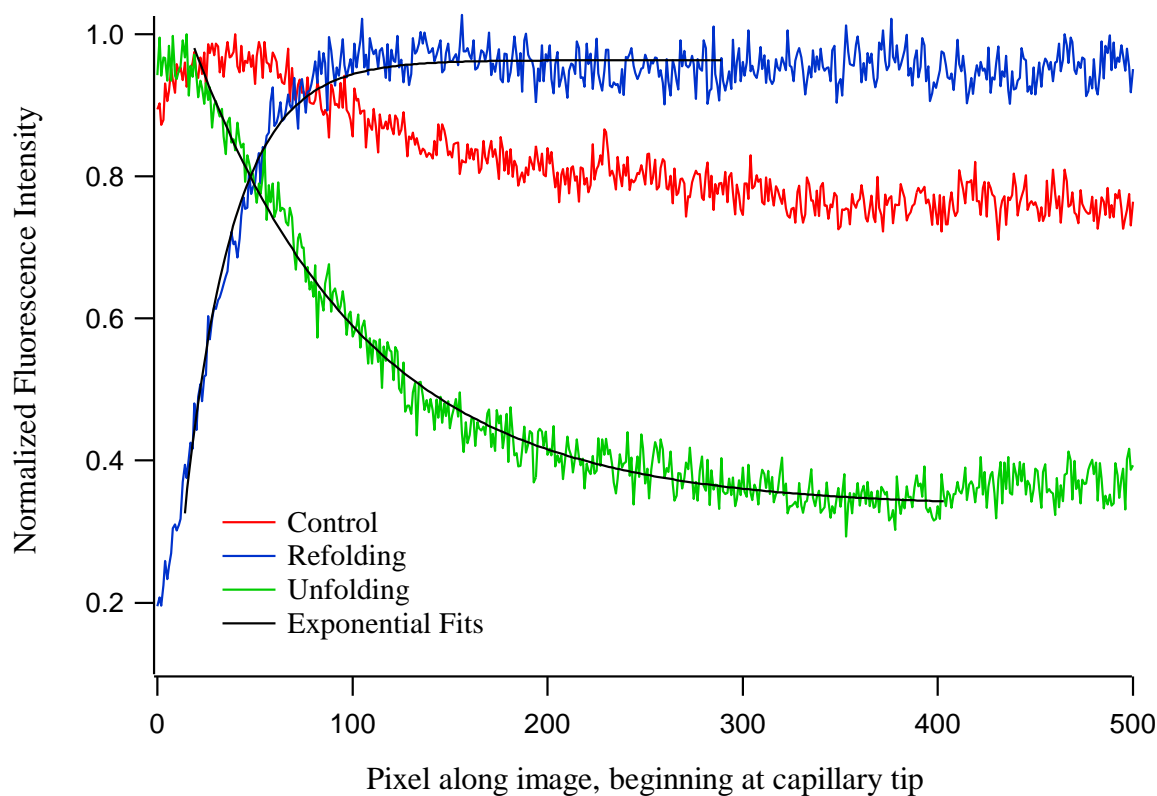
Figure 15. Changes in fluorescence intensity of apoMb: 1,8-ANS sample due to changes in apoMb conformation as the protein experiences changes in pH.

Table 2. Variables and Final Equation for Exponential Fits of apoMb Folding Data

Variable	Unfolding Data	Refolding Data
y_0	0.33459 ± 0.00275	0.96338 ± 0.00199
A	0.8026 ± 0.00813	-1.1214 ± 0.031
invTau	0.011457 ± 0.000217	0.040348 ± 0.00106
Final Equation	$y = 0.33459 + 0.8026e^{-0.011457}$	$y = 0.96338 - 1.1214e^{-0.040348}$
Reaction Time, µs	607	172

The data presented here are unique from that obtained from other apoMb folding experiments. Because the data fit to single exponential functions, a transition between only two states (rather than three or four) was observed in both the unfolding and refolding experiments. The reaction times reported here are also different from those found in other studies. The data may be best explained by considering the possible energy landscape of apoMb folding.

In the introduction, protein folding was described as the progression of a protein's structure from being a linear chain of amino acids to a 3D complex. The process often involves a protein attaining one or more intermediate states between its initial and final structures, but the actual mechanism of folding is still largely unknown. One way to describe the mechanism is by considering the relative free energies of each conformation that a protein accesses while folding. The unfolded protein has the highest free energy, and the folded protein in its native state has the lowest free energy. Overall then, folding is driven by a tendency to decrease free energy. As a protein's free energy is lowered, the number of conformations available to the protein is decreased. The protein eventually reaches a minimum free energy where only one conformation is possible – the native state (Figure 16) [31].
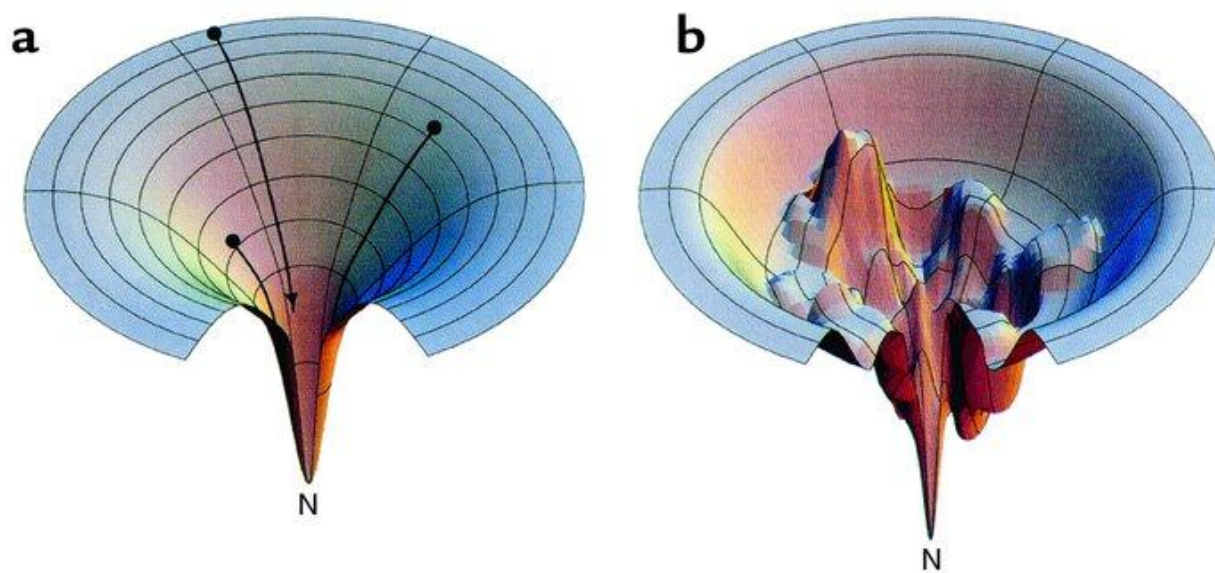
Figure 16. Energy landscape diagrams for protein folding, adapted from Horwich, 2002 [31]. N stands for the native state. (a) shows a smooth landscape with no energetic barriers. Folding in this case may proceed directly from a relatively high-energy unfolded structure to the native state. (b) shows a rough landscape with energetic barriers represented by local maxima and minima in free energy. Folding in this case may involve one or more high-energy transition states or low-energy intermediate states before reaching the native state.

The shape, or roughness, of the energy landscape dictates how a protein will fold. Figure 16 part (a) shows a smooth landscape, while part (b) shows a rough landscape. Both demonstrate that a protein may follow a large number of different paths to reach its native state. As a protein lowers its free energy and proceeds down these landscapes, it may encounter certain barriers that affect folding. Such barriers appear in the topology of the rough landscape diagram. The local maxima are energy barriers that a protein must overcome to continue down a certain pathway, and the local minima are traps where the protein may adopt a fairly stable conformation. During folding, a free energy maximum corresponds to a relatively high-energy transition state, and a free energy minimum corresponds to a relatively low-energy intermediate state [31]. A given trajectory down the energetic funnel outlines a folding pathway with a unique number of conformational transitions and intermediate states.

Considering the free-energy-landscape description of protein folding, the unfolding of apoMb is expected to require more time than refolding, since the latter involves an unfavorable increase in free energy. Our data is consistent with this trend: we observed an unfolding time that was approximately 3.5 times longer than the folding time. However, the states that apoMb transitions between are not completely understood. The single-exponential behavior of our protein folding data supports that apoMb undergoes a transition between two distinct conformations, although the widely accepted mechanism of apoMb folding involves transitions between four possible states (Figure 17). The nature of the transitions we observed most likely result from altering the energy landscape of apoMb such that two states are highly favored over

the others. Certain energetic barriers may have been lowered or eliminated by inducing folding with rapid pH changes.

In the unfolding experiment, apoMb began at a pH of approximately 5.5, at which the protein is expected to be in its N form [26, 32]. The unfolding experiment therefore involves a single transition of apoMb from its N form to one of its less-ordered forms. The possible transitions include N to I, N to E, or N to U. The N to I transition is possible because the I form, though able bind and enable the fluorescence of 1,8-ANS, does not bind 1,8-ANS as strongly as the N form does. Hence, the fluorescence intensity of the I form is diminished in comparison to the N form. In the refolding experiment, apoMb began at a pH of approximately 3, at which the protein is in its U form [26]. The possible transitions include U to I or U to N. The transition from U to E is unlikely because the E form is too loosely structured to properly bind 1,8-ANS. Analyzing the measured times of unfolding and folding may help determine which transitions were actually observed.

The refolding time of 172 μs agrees with other measured times for apoMb folding from its U to N form. These other studies measured folding times of 100 – 300 μs [21, 32]. This gives evidence that the observed unfolding pathway involved a direct transition of apoMb from U to N. Based on this conclusion, the energy landscape created by the large pH gradient of our experiments seems to favor a folding pathway that lacks an intermediate state. If so, then the unfolding reaction observed may also involve a transition between the N and U forms of apoMb. In our experiments, the I state of apoMb seems to have been bypassed or was not sufficiently stabilized such that apoMb could populate this state for a noticeable period of time. Because the extreme pH conditions largely favor the N state (at pH 5 or above) or U state (at pH 3 or below), this apparent loss of the intermediate state is plausible [26]. However, the measured times, and

therefore predicted transitions, may not be completely correct because of error in the calibration data. To further support our conclusion that apoMb transitions between its N and U forms, experiments that are predicted to access other forms of apoMb should be conducted. The I form of apoMb is stabilized at a pH of 4 [26], so adjusting the pH of apoMb to this level (instead of 2 or 6-7 as we did in the unfolding and refolding experiments, respectively) may cause transitions that bring apoMb to its I form. If unfolding and refolding experiments that achieve an ultimate pH of 4 show smaller changes in fluorescence intensity than the experiments conducted here, then we may more confidently conclude that the experiments of this study involved transitions between the N and U forms of apoMb. If the experiments reaching a pH of 4 demonstrated fluorescence intensity changes very similar to those observed in this study, then these results may actually reflect transitions between the N, I, and U forms of apoMb. Such studies that investigate smaller pH changes will be pursued in future investigations.

Although the 172-μs folding time of apoMb reported here agrees with that determined in some other studies, it does not agree with the times measured in all apoMb experiments. In general, our measured unfolding and refolding times differ from those found in the literature [5, 33, 34]. Furthermore, many of these literature sources report apoMb folding times that are not in agreement with one another. For instance, in Figure 17, the folding time of 24 ms for the transition between I and N is much longer than the folding time observed in this study and was calculated from sources reporting different folding times. The calculation involved extrapolating data from two different experiments – one conducted at 60°C (giving a folding time of 280 μs) and the other at 5°C (giving a folding time of 1 s) – to determine a theoretical folding time for apoMb at 35°C [5]. Based on all the results mentioned above, apoMb folding can occur over a large range of different times.
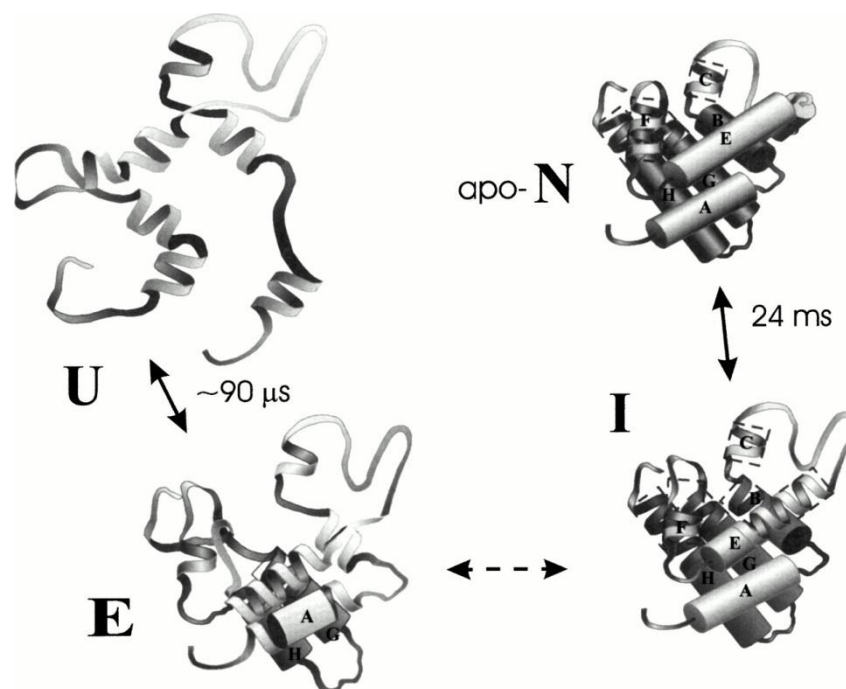
Figure 17. Schematic of apoMb folding from its U →E→I→N forms, adapted from Callender *et al*., 1998 [5]. The times reflect folding, rather than unfolding, events. The rate of the E→I transition is not known.

The many different results for apoMb's folding kinetics reveal that the protein's folding pathway is not fixed. Rather, this pathway varies based on how an experiment is conducted. Changing the protein environment and even using a different method to observe folding seem to alter the mechanism itself. For example, the transition between the U and E conformations of apoMb has been shown to proceed through more than two unique folding routes when IR absorbance versus Trp fluorescence studies were conducted [34]. In this study, rapidly lowering the pH of apoMb's environment by simply introducing or removing protons favored fast transitions between two distinct states. Creating a comprehensive folding diagram for apoMb, as well as other proteins, requires the synthesis of data obtained from using a wide variety of techniques. From such diagrams, general patterns and rules of protein folding could be inferred.

The question of how a protein folds may have a large number answers, but with a set of rules to describe protein behavior under given conditions, those answers could be reached.

4. CONCLUSION

The purpose of this study was to develop a microfluidic fast mixer for protein folding studies. The mixer was first characterized by calibrating its time resolution and diffusional mixing time. Some error in these calculations may have resulted from the inner capillary being displaced from the exact center of the outer capillary. As a result, the focus of the microscope may not have been on the center of the sample stream. These errors could be corrected with mechanical adjustments to prevent bending of the inner capillary and use of the microscope's spinning disk to determine the center of the sample stream. Nonetheless, the experimental data for mixer characterization was applied to a final experiment on protein folding. ApoMb was unfolded and refolded within the mixer via a decrease and increase, respectively, of the protein's environment in the absence of buffer. The folding reactions involved a single transition between two states of the protein, even though the protein has been shown to populate four different conformations during its folding pathway. The conditions of this experiment may have altered the energy landscape of apoMb such that two distinct states are highly favored over the others. By comparing the data to other studies, the folding reactions seemed to involve the N and U forms of apoMb, meaning the I form was bypassed or was not be populated for a significant amount of time under the conditions of our experiments. Because of the strong dependence of folding mechanisms and rates on external conditions, compiling data collected from many different types of experiments is necessary to fully understand protein folding. In this comprehensive protein folding scheme, which would include studies probing such effects as

temperature jumps, denaturant concentration variations, and pump-probe pulses [5], our

technique contributes the effect of rapid pH changes on protein structure dynamics.

REFERENCES

1. Karplus, Martin, Andrej Sali, and Christopher M. Dobson. Protein Folding: A Perspective from Theory and Experiment. 1998. *Angew. Chem. Int. Ed.* 37: 868-893.
2. Newton, Alexandra C. 1995. Protein Kinase C: Structure, Function, and Regulation. *J Biol Chem*. 270: 28495-28498.
3. Lee, Cheolju and Myeong-Hee Yu. Protein Folding and Diseases. 2005. *J. Biochem. and Molec. Biol.* 38: 275-280.
4. Epstein, Charles J., Robert F. Goldberger, and Christian B. Anfinsen. 1963. The Genetic Control of Tertiary Protein Structure: Studies of Model Systems. *Cold Spring Harb Symp Quant Biol*. 28: 439-449.
5. Callender, Robert H., R. Brian Dyer, Rudolf Gilmanshin, and William H. Woodruff. Fast Events in Protein Folding: The Time Evolution of Primary Processes. *Annual Review of Physical Chemistry*, 1998, **49**: 173-202.
6. Eaton, William A., Peggy A Thompson, Stephen J Hagen, and James Hofrichter. 1996. Fast Events in Protein Folding. *Structure.* 4: 1133-1139.
7. Beebe, David J., Glennys A. Mensing, and Glenn M. Walker. 2002. Physics and Applications of Microfluidics in Biology. *Annu. Rev. Biomed. Eng.* 4: 261-86.
8. Nguyen, Nam-Trung and Zhigang Wu. 2005. Micromixers – a review. *J. Micromech. Microeng.* 15: R1-R16.
9. Knight, James B., Ashin Vishwanath, James P. Brody, and Robert H. Austin. 1998. Hydrodynamic Focusing on a Silicon Chip: Mixing Nanoliters in Microseconds. *Phys. Rev. Lett*. 80: 3863-3866.
10. Pabit, Suzette A. and Stephen J. Hagen. 2002. Laminar-Flow Fluid Mixer for Fast Fluorescence Kinetic Studies. *Biophys. J*. 83: 2872-2878.
11. Hertzog, David E, Xavier Michalet, Marcus Jager, Xiangxu Kong, Juan G. Santiago, Shimon Weiss, and Olgica Bakajin. 2004. Femtomole Mixer for Microsecond Kinetic Studies of Protein Folding. *Anal. Chem.* 76: 7169-7178.
12. Hertzog, David E., Benjamin Ivorra, Bijan Mohammadi, Olgica Bakajin, and Juan G. Santiago. 2006. Optimization of a Microfluidic Mixer for Studying Protein Folding Kinetics. *Anal. Chem.* 78: 4299-4306.
13. Park, Yoon Hye, Xiangyun Qiu, Elizabeth Rhoades, Jonas Korlach, Lisa W. Kwok, Warren R. Zipfel, Watt W. Webb, and Lois Pollack. 2006. Achieving Uniform Mixing in a Microfluidic Device: Hydrodynamic Focusing Prior to Mixing. *Anal. Chem*. 78: 4465-4473.
14. Yao, Shuhuai and Olgica Bakajin. Improvements in Mixing Time and Mixing Uniformity in Devices Designed for Studies of Protein Folding Kinetics. 2007. *Anal. Chem.* 79: 5753-5759.
15. Hamadani, Kambiz M. and Shimon Weiss. 2008. Nonequilibrium Single Molecule Protein Folding in a Coaxial Mixer. *Biophys. J.* 95: 352-365.

16. Gamin, Yann, Claire Simonnet, Virginia VanDelinder, Ashok Deniz, and Alex Groisman. 2009. Ultrafast microfluidic mixer with three-dimensional flow focusing for studies of biochemical kinetics. *Lab Chip*. 10: 598-609.

17. 17. Royer, Catherine A. 2006. Probing Protein Folding and Conformational Transitions with Fluorescence. *Chem. Rev.* 106: 1769−1784

18. Gräf, Ralph, Jens Rietdorf, and Timo Zimmerman. 2005. Live Cell Spinning Disk Microscopy. *Adv. Biochem. Eng/Biotechnol.* 95: 57-75.

19. Conchello, José-Angel and Jeff W Lichtman. 2005. Optical Sectioning Microscopy. *Nature Methods*. 2: 920-931.

20. Pollack, Lois, Mark W. Tate, Nicholas C. Darnton, James B. Knight, Sol M. Gruner, William A Eatons, and Robert H. Austin. Compactness of the denatured state of a fast-folding protein measured by submillisecond small-angle x-ray scattering. 1999. *Proc. Natl. Acad Sci. USA*. 96: 10115-10117.

21. Lapidus, Lisa J., Shuhuai Yao, Kimberly S. McGarrity, David E. Hertzog, Emily Tubman, and Olgica Bakajin. 2007. Protein Hydrophobic Collapse and Early Folding Steps Observed in a Microfluidic Mixer. *Biophys J.* 93: 218-224

22. Toepke, Michael W., Scott H. Brewer, Dung M. Vu, Kirk D. Rector, Joel E. Morgan, Robert B. Gennis, Paul J. A. Kenis, and R. Brian Dyer. 2007. Microfluidic Flow-Flash: Method for Investigating Protein Dynamics. *Anal. Chem.* 79: 122-128.

23. Uzawa, Takanori, Shuji Akiyama, Tetsunari Kimura, Satoshi Takahashi, Koichiro Ishimori, Isao Morishima, and Tetsuro Fujisawa. 2004. Collapse and search dynamics of apomyoglobin folding revealed by submillisecond observations of α-helical content and compactness. *Proc. Natl. Acad. Sci. USA*. 101: 1171-1176.

24. Weisbuch, Sebastian, Francine Gérard, Marielle Pasdeloup, Jérémy Cappadoro, Yves Dupont, and Marc Jamin. 2005. Cooperative Sub-Millisecond Folding Kinetics of Apomyoglobin pH 4 Intermediate. *Biochemistry*. 44: 7013-7023.

25. Meinhold, Derrick and Peter E. Wright. 2011. Measurement of protein unfolding/refolding kinetics and structural characterization of hidden intermediates by NMR relaxation dispersion. *PNAS*. Early edition: 1-6.

26. Yange, An-Suei and Barry Honig. 1994. Structural Origins of pH and Ionic Strength Effects on Protein Stability: Acid Denaturation of Sperm Whale Apomyoglobin. *J. Mol. Biol.*237: 602-614.

27. Fancolli, Ted M. and Salvatore F. Russo. 1970. Interaction of a Naphthalene Dye with Apohemoglobin. *J. Chem. Ed.* 47: 54-55.

28. Tsien, Roger Y., Lauren Ernst, and Alan Waggoner. *Handbook of Biological Confocal Microscopy, Third Edition.* "Fluorophores for Confocal Microscopy: Photophysics and Photochemistry." 2006.

29. Adams, P.A. 1977. The Kinetics of Recombination Reaction between Apomyoglobin and Alkaline Haematin. *Biochem. J.* 163: 153-158.

30. Weber, Gregorio and Lorna B. Young. 1964. Fragmentation of Bovine Serum Albumin by Pepsin: I. The origin of the acid expansion of the albumin molecule. *J Biol Chem*. 239: 1415-1423.

31. Horwich, Arthur. 2002. Protein aggregation in disease: a role for folding intermediates forming specific multimeric interactions. *J Clin Invest.* 110: 1221-1232.

32. Gilmanshin, Rudolf, Skip Williams, Robert H. Callender, William H. Woodruff, and R. Brian Dyer. 1997. Fast events in protein folding: Relaxation dynamics of secondary and tertiary structure in native apomyoglobin. *PNAS*. **94**: 3709-3713.

33. Meinhold, Derrick W. and Peter E. Wright. 2011. Measurement of protein unfolding/refolding kinetic and structural characterization of hidden intermediates by NMR relaxation dispersion. *PNAS*. **108**: 9078-9083.

34. Gulotta, Miriam, Rudolf Gilmanshin, Thomas C. Buscher, Robert H. Callender, and R. Brian Dyer. 2001. "Core Formation in Apomyoglobin: Probing the Upper Reaches of the Folding Energy Landscape. *Biochemistry*. 40: 5137–5143.